Article

Fabrication and Characterization of Inverse-Opal Titania Films for Enhancement of Photocatalytic Activity

Lei Wang, Tharishinny R. Mogan, Kunlei Wang [ID], Mai Takashima [ID], Bunsho Ohtani [ID] and Ewa Kowalska *[ID]

Institute for Catalysis (ICAT), Hokkaido University, Sapporo 001-0021, Japan; wang.lei@cat.hokudai.ac.jp (L.W.); rajamogan.t@cat.hokudai.ac.jp (T.R.M.); kunlei@cat.hokudai.ac.jp (K.W.); takashima.m@cat.hokudai.ac.jp (M.T.); ohtani@cat.hokudai.ac.jp (B.O.)
* Correspondence: kowalska@cat.hokudai.ac.jp

Abstract: Novel materials with a periodic structure have recently been intensively studied for various photonic and photocatalytic applications due to an efficient light harvesting ability. Here, inverse opal titania (IOT) has been investigated for possible enhancement of photocatalytic activity. The IOT films were prepared on a glass support from silica and polystyrene (PS) opals by sandwich-vacuum-assisted infiltration and co-assembly methods, respectively. The reference sample was prepared by the same method (the latter) but with PS particles of different sizes, and thus without photonic feature. The modification of preparation conditions was performed to prepare the films with a high quality and different photonic properties, i.e., photonic bandgap (PBG) and slow photons' wavelengths. The morphology and optical properties were characterized by scanning electron microscopy (SEM) and UV/vis spectroscopy, respectively. The photocatalytic activity was evaluated (also in dependence on the irradiation angle) for oxidative decomposition of acetaldehyde gas under irradiation with blue LED by measuring the rate of evolved carbon dioxide (CO_2). It has been found that PBG wavelength depends on the size of particles forming opal, the void diameter of IOT, and irradiation angle, as expected from Bragg's law. The highest activity (more than two-fold enhancement in the comparison to the reference) has been achieved for the IOT sample of 226-nm void diameter and PBG wavelengths at 403 nm, prepared from almost monodisperse PS particles of 252-nm diameter. Interestingly, significant decrease in activity (five times lower than reference) has been obtained for the IOT sample of also high quality but with 195-nm voids, and thus PBG at 375 nm (prohibited light). Accordingly, it has been proposed that the perfect tunning of photonic properties (here the blue-edge slow-photon effect) with bandgap energy of photocatalyst (e.g., absorption of anatase) results in the improved photocatalytic performance.

Keywords: photocatalysis; photonic crystals; inverse opal; titania

1. Introduction

Photocatalysis is considered as possible solution for emerging threats facing humanity, such as energy shortage, environmental pollution, and deficiency of drinking water [1]. Photocatalysts are materials, which are excited under photoirradiation, and thus formed charge carriers (electrons and holes) might either start chemical reactions, including "green" fuels' formation [2], and decomposition of organic [3], inorganic [4], and microbiological [5] pollutants or directly be used as photo-current (photogenerated electrons) [6]. However, in the case of semiconductor photocatalysis, the recombination of charge carriers often results in insufficient quantum yields for commercial application [7,8]. Moreover, the most active photocatalysts are characterized by wide bandgap, and thus UV light must be used for their excitation. Accordingly, only small portion of solar radiation (the most recommended source of irradiation for "green" and cheap technology) could be efficiently use for photocatalytic reactions. In this regard, various strategies have been proposed to obtain highly efficient solar photocatalysts, including modification of wide-bandgap

semiconductors (doping [9–11], surface modification [12–14], and heterojunction [15–17]) and development of novel photocatalytic systems in the form of both single [18–22] and multi-element (e.g., Z-scheme [23–25]) materials.

There are two essential components of photocatalysis: (i) the photoabsorption initiated by photoirradiation, and (ii) the chemical reactions begun by photogenerated charge carriers. Although many studies have been performed to obtain vis-responsive materials, most efforts on the improvement of photocatalytic performance have been focused on the inhibition of charge carriers' recombination since photoabsorption efficiency is usually uncontrollable as fixed physical property of photoabsorbing materials. Accordingly, a common strategy for enhancing the photocatalytic activity of semiconductor photocatalysts is to enhance the quantum efficiency, by accelerating the surface reaction [26] and/or hindering the charge carriers' recombination [27], e.g., by spatial charge separation [28–32]. However, quantum efficiency might be enhanced maximally to 100% (despite special cases, e.g., when formed products can further transfer charge carriers via photoinduced bi-electronic transfer mechanism [33]) and further enhancement is not expected. Another, but negligibly employed strategy is to enhance photoabsorption efficiency. One of the possible ways for photoabsorption enhancement beyond fixed photoabsorption coefficient is to use slow photon effect, which appears at photonic bandgap (PBG) edges in photonic crystals (PCs), such as inverse opal (IO) structures [34–36].

The PCs are materials of a periodic arrangement that affects the motion of photons. The uniqueness of PCs is photonic bandgap (PBG), wherein the light of particular frequency cannot propagate through the material, whereas the light of wavelengths near PBG can propagate, but with strongly reduced group velocity [37–39]. This phenomenon is so-called slow photon effect. The existence of PBG and slow photon effect causes the beautiful coloration of matters (e.g., butterflies and mineral opals) and makes possible to trap the light inside materials for amplified light harvesting. The most common PC is IO structure [36,39–41], i.e., an inverse replica of the opal template in the face-centered-cubic (FCC) arrangement. Various materials have already been synthesized in the form of both opal and IO structures, including also one of the most famous photocatalysts—titania [42–44]. By applying the IO PCs structure to titania, the enhanced photoabsorption of light is expected due to the extended light-path length owing to the slow photon effect, as already confirmed in some studies [34–36].

Different forms of IO PCs could be prepared depending on the intended application, including the most common two-dimensional (2D) films and three-dimensional (3D) particles. In the case of 2D structures, typically, the fabrication of inverse opal titania (IOT) on the glass support is composed of five main steps: (1) the synthesis of colloidal nanoparticles (NPs), (2) the preparation of an opal template built from spherical NPs on the glass support, (3) the infiltration of titania precursor to form the framework, (4) the phase transfer from amorphous into crystalline forms of titania (anatase or rutile), and (5) the removal of an opal template. The infiltration process is critical because it results in the formation of the main framework of titania. Generally, dip coating [45] and drop casting [46] are commonly used for the infiltration. However, overlayers are easily formed on the bulk titania due to the excess of titania precursor [47]. Hence, vacuum-assisted sandwich method [48,49] has been used in this study to avoid the formation of overlayers. Additionally, co-assembly method has been investigated to obtain continuous IOT films with a high quality and different photonic properties. Accordingly, the property-governed activity might be studied and the strategy on the preparation of highly efficient photocatalysts could be proposed. The main purpose of this study is to check if and how the tunning of the photonic properties might influence the photocatalytic properties.

2. Materials and Methods

2.1. Materials

Titanium tetraisopropoxide (TTIP), tetraethyl orthosilicate (TEOS), 25% ammonia solution, 15% tetramethylammonium hydroxide solution (TMAH), 30% hydrogen peroxide, sulfuric acid, sodium hydroxide, potassium hydroxide, 2-propanol, and 99.5% ethanol were purchased from FUJIFILM Wako Pure Chemical, potassium persulfate (KPS) and styrene were purchased from SIGMA-ALDRICH and used without further treatment. Milli-Q water with a resistivity of 18.2 MΩ was used during experiments.

Glass (support for IOT) used in this study was pretreated to make its surface hydrophilic by immersing glass slides in piranha solution (H_2O_2 and H_2SO_4 in the ratio of 2:3) and 1 M of KOH solution for 15 min each [50].

2.2. Fabrication of Inverse Opal Titania via Infiltration Method

The IOT samples were prepared via following steps: (1) Silica colloidal particles were synthesized via Stober method [51]; (2) Then, silica opals were formed on the pretreated glass slides via evaporation, where induced self-assembly was achieved by immersing pretreated glass in 1 wt.% silica ethanol suspension nearly vertically. Vials containing glass and silica suspension were heated at 40 °C in a drying oven. The deposition of silica opals on glass took three days; (3) The formed opals were covered with additional glass, fixed by clips to make a sandwich-like structure (to avoid the formation of overlayers [48,49]). Then, titania precursor (10 vol% TTIP in ethanol) was infiltrated into the interstitial spaces between silica particles, and exposed to air (to form amorphous titania); (4) Amorphous titania was crystallized into anatase in the electric furnace at 500 °C for 2 h with ramping at 0.5 degrees/min; (5) Finally, the opal template was removed by dipping the silica/titania composite film in hot NaOH solution (1 M). The obtained samples were named respectively to the silica particles diameter, e.g., opal-200 means that the sample was composed of 200-nm silica particles.

2.3. Fabrication of Inverse Opal Titania via Co-Assembly Method

The co-assembly method follows the main fabrication process described above (Section 2.2.), i.e., opal formation, titania infiltration, and opal removing. However, co-assembly method [52] is simpler than infiltration one, since the opal template and titania are deposited on the glass simultaneously (one step), and crystallization of titania and removal of opal are proceeds also in one step. Accordingly, co-assembly method consists of only three steps as follows: (1) synthesis of polystyrene (PS) particles, (2) co-assembly (opal formation from PS and titania deposition within the opal), and (3) removal of opal and titania crystallization. The pre-synthesized titania was prepared according to the literature [52]. In brief, 1.1 mL of TTIP was added to 15 mL of 2-propanol and stirred for 10 min, while 1.38 g TMAH (15%) was added to 180 mL of water in a flask immersed in an ice bath. Then, TTIP in 2-propanol was introduced dropwise to the cooled TMAH solution under continuous stirring. Then 10 min later, the flask was transferred to a mineral oil bath and heated at 100 °C for 6 h. The co-assembly is based on the evaporation induced self-assembly (the same idea as in the case of the infiltration method). The aqueous suspension of PS (0.1 wt%) was mixed with titania suspension (titania to 2-propanol—1:10) in a small vial. Then, the clean glass slide was immersed in the vial almost vertically, and then heated at 65 °C to form the PS(opal)/titania composite film. The IOT crystalline film on the glass was obtained by heating the glass in an electric furnace at 500 °C for 2 h (crystallization of titania to anatase and removal of PS opal template). The samples were named respectively to the void diameter, e.g., IOT with voids of 156 nm was named as IOT-156.

In addition, the porous titania film on a glass substrate was prepared as a reference sample. The reference was fabricated using the same procedure as that used for the preparation of IOT samples from PS opal, but three kinds of PS particles (PS diameter of 195, 226, and 246 nm; volume ratio of 1:1:1) were used. Accordingly, the reference was characterized by similar surface properties to IOT samples but without PBG feature.

2.4. Characterization

The morphology of opal and IOT films was characterized by LV-SEM and FE-SEM. The transmittance spectra of IOT films were measured with JASCO V-670 spectrophotometer (JASCO V-670). The photocatalytic activity of IOT samples was evaluated with oxidative decomposition of acetaldehyde gas under aerobic conditions by measuring the rate of evolved carbon dioxide (CO_2) using GC-FID. The IOT sample immersed in 66-mL quartz cell containing 1.5 mL of acetaldehyde was irradiated with UV LED (λ = 365 nm; 0.28 W; photoemission spectra shown in Figure 1). The influence of irradiation angle was also investigated in the range from 0° to 40°, while the distance between the light source and the sample film was fixed at 4 cm.
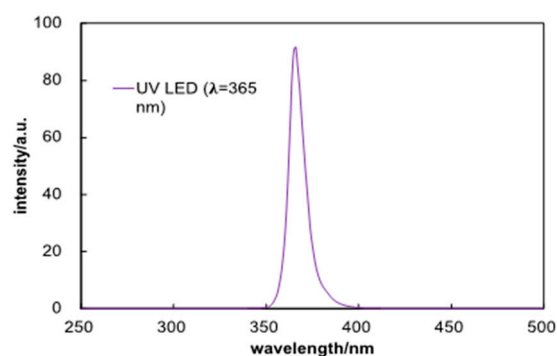
Figure 1. Photoemission spectra of UV-LED used in photocatalytic activity tests.

The photonic bandgap (PBG) has been estimated by using a modified Bragg's equation, shown below:

$$\lambda_{max} = 1.632D \sqrt{n_{avg}^2 - sin^2\theta} \tag{1}$$

where λ_{max} is the wavelength of the band maximum, D is the diameter of spheres, and θ is the angle between incident beams and plane. The average refractive index n_{avg} can be calculated using following equation:

$$n_{avg} = fn_{sphere} + (1 - f)n_{air} \tag{2}$$

where f is the filling factor of spheres and n is the refractive index of materials. According to the theoretically calculated PBG, the size and/or the angle dependent PBG wavelength is expected.

3. Results and Discussion
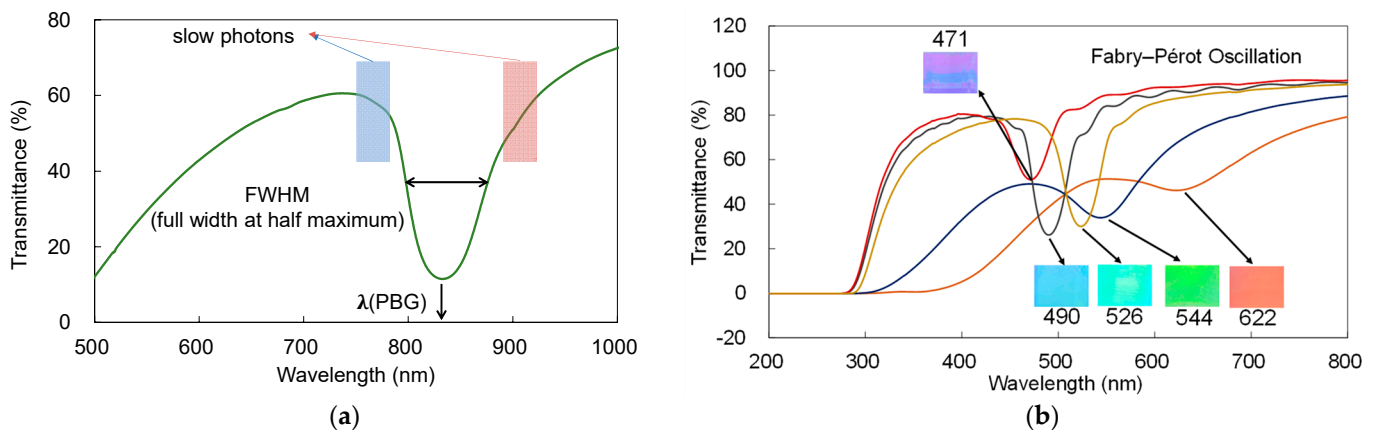
3.1. Characterization of Opals

The successful preparation of opals and respective inverse opals could be easily observed by intensive coloration of samples, as well as the change of colors in dependence on the observation angle. Indeed, all prepared samples have been colored, and the viewing angle influences the observable color, as exemplary shown in Figure 2a. The respective IOT film prepared by infiltration route is presented in Figure 2b. Of course, the microscopic observations have confirmed the formation of ordered structures for both opal and inverse opal materials, as shown in Figure 2c,d (silica diameter of 393 nm and the corresponding void diameter of 292 nm, respectively). Accordingly, it has been shown that well-ordered structure of both opal and IOT could be formed by the infiltration method. However, as shown in Figure 2b, IOT has not been formed on the whole surface of glass (part of the film in red), indicating the incomplete infiltration of opal with titania.
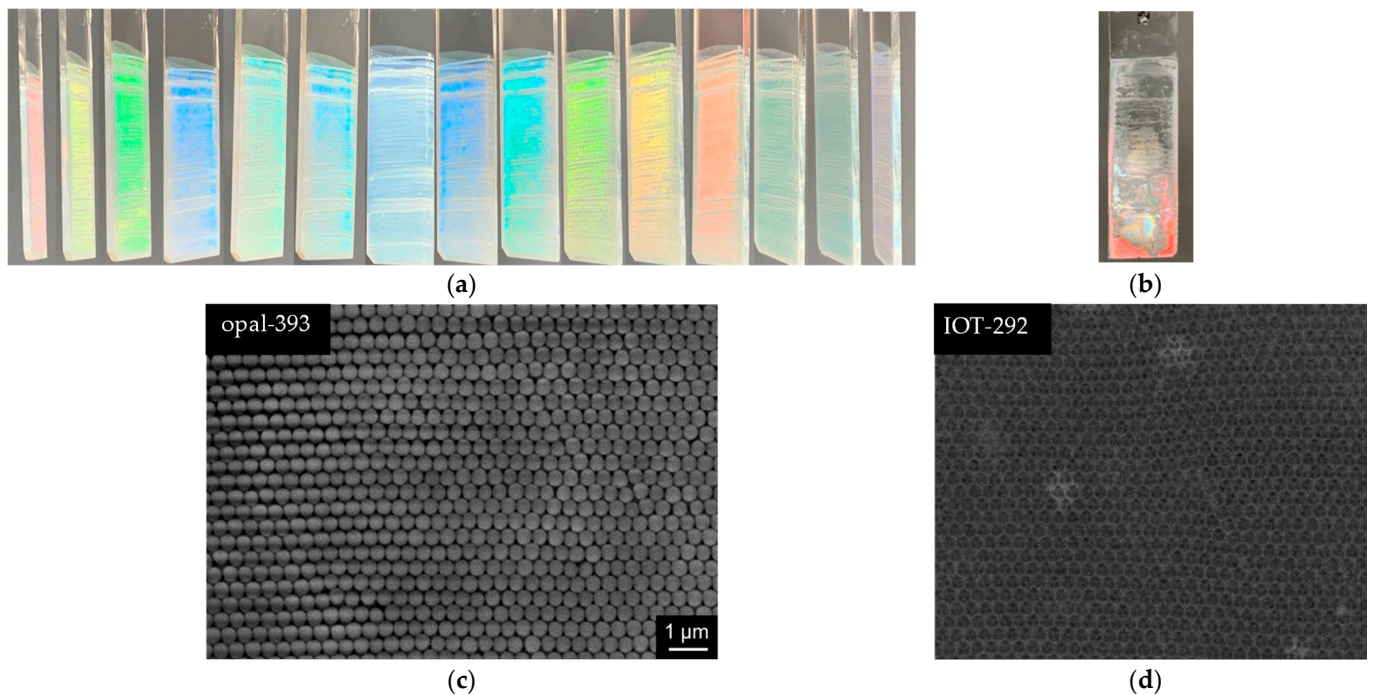
Figure 2. (**a**) The color changes of silica opal film (opal-393) with different observation angle and (**b**) corresponding IOT (IOT-292); (**c**) SEM image of opal with silica diameter of 393 nm and (**d**) corresponding IOT with pore diameter of 292 nm.

It should be pointed out that the formation of closely packed opal with minor defects is a necessary condition to fabricate IOT PCs of a good quality. A series of silica opal samples with different diameter of silica particles (471, 490, 526, 544, and 622 nm) has been successfully synthesized with minimum size/shape variation of 5%. Figure 2c confirms the closely packed silica spheres' array in face-centered cubic arrangement with almost no cracks (probably caused by drying [36]).

To investigate optic properties of opals and inverse opals, PBG should be estimated (as shown in Figure 3a), and thus transmittance spectra have been taken for all samples. Moreover, the expected wavelengths of slow photons at both edges (blue and red) of PBG (Figure 3a), and the quality of opal/inverse opal (besides microscopic observations) could also be obtained from transmission spectra. The full width at half maximum (FWHM) of PBG peak (Table 1) indicates the quality, i.e., the smaller the value is, the higher is the quality.

Figure 3. (**a**) The characterization of optical properties of PCs based on transmittance spectrum; (**b**) transmittance spectra and respective photos of silica opals with different sizes of silica particle (PBG wavelengths written near photos).

**Table 1.** Properties of silica opals with different silica sizes.

	opal-210	opal-220	opal-240	opal-250	opal-300
D (SiO_2)/nm	210	220	240	250	300
experimental λ_{opal}/nm	471	490	526	544	622
calculated λ_{opal}/nm	487	510	557	580	696
FWHM/nm	43	38	40	55	55

PBG is strongly influenced by the spheres' diameter (opal) and the angle of the light penetrating the structure. Accordingly, it could be observed that PBG wavelength varies in dependence on the silica diameter, as shown in Figure 3b. The bathochromic shift has been found with an increase in silica diameter, as expected from the Brag's law.

Moreover, the smaller values of FWHM for opals built from smaller silica particles confirm the high quality of these opals due to high monodispersity. In contrast, opals with larger silica particles (250 and 300 nm), characterized by much wider PBG peak, are more polydisperse (with some variation in the silica sizes). Unfortunately, it is almost impossible to obtain opals with monodisperse large silica particles since large particles lead to the high dispersity due to the growth of additional silica seeds.

Additionally, smaller peaks (Figure 3b), known as Fabry–Perot fringes, have been observed for opal-210, opal-220, and opal-240, which could arise from the multiple reflections of light at the interfaces in PCs [53]. It should be highlighted that the calculated PBG wavelengths (Brag's law) correspond well to the experimental values, indicating a good quality of the formed opal structures.

As already mentioned (Figure 3a), the angle of irradiation strongly affects the PBG characteristics of PCs. Indeed, extinction spectra taken for one opal structure at different angle of irradiation confirm significant differences in the position of PBG peaks. Here, hypsochromic shift has been observed with an increase in the irradiation angle (Figure 4), as expected from Brag's law. This could be explained by the diffraction of light passing the multiple layers of the opal structure, which results in color changing with the change in the angle of irradiation.
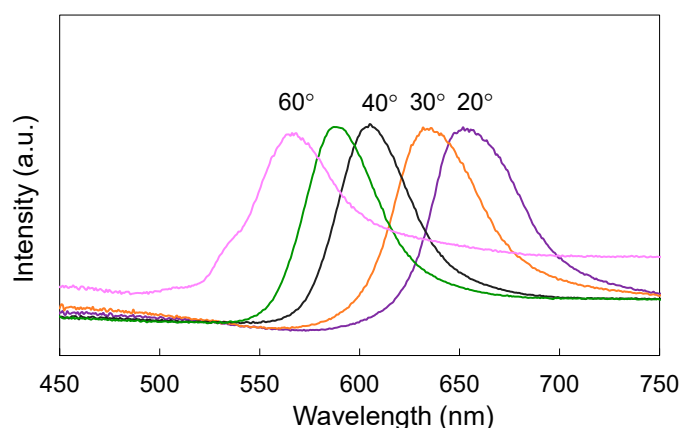
Figure 4. Angle dependance of PBG for silica opal (opal-295).

3.2. Characterization of Inverse Opal Titania

Infiltration of titania (or its precursor) inside opal structure is the most challenging and critical step during the formation of IOT of a good quality. Unsuccessful infiltration or low filing ratio result in a lack or incomplete PBG peak, and thus disrupting the photonic effect. Accordingly, two methods have been applied to obtain the IOT film samples of a high quality. Firstly, the direct infiltration assisted with sandwich-vacuum method was applied to allow the titania precursor to fill in the interstices voids of the opal structure. Figure 5 presents IOT samples with different void sizes after the removal of the silica template. Unfortunately, the quality of almost all IOT samples (except that shown in Figure 2d) is

not good, as some cracks and irregular size of the voids are clearly observed. This could be explained by the excessive titania precursor penetration into the voids and the fast hydrolysis and condensation, which leads to excessive formation of titania. The presence of oxygen on the opal film prior the infiltration could be another factor that leads to the formation of irregular IOT structure. However, the sample of IOT-292 of a good quality has been successfully synthesized from the opal template of 393-nm size (Figure 2c), as presented in Figure 2d. Probably, the largest sizes of silica (here 393 nm) could be the optimum for the perfect infiltration of titania precursor.
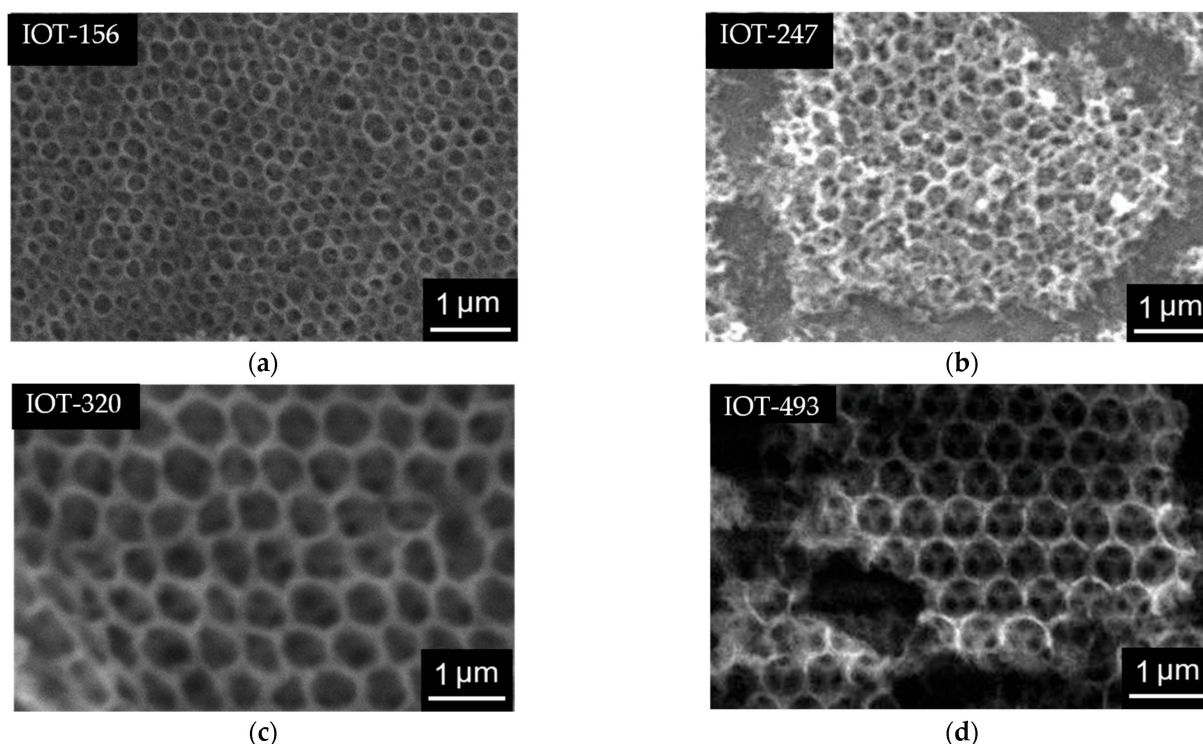
Figure 5. SEM images of: (**a**) IOT-156; (**b**) IOT-247; (**c**) IOT-320; (**d**) IOT-493.

The shrinkage of voids (Table 2), in the comparison to the original diameter of silica particles forming opal, has been observed in all samples due to the calcination process, which agrees with the previous reports [34,54–56]. As expected, no PBG peaks could be observed in transmittance spectra due to the poor and irregular formation of titania, except for IOT-292 sample, showing PBG at 647 nm (Table 2). Overall, it has been concluded that it is hardly possible to obtain large-scale, well-ordered IOT films of different properties (PBG and slow photons) by the infiltration method. Hence, another approach has been tried, i.e., the co-assembly method.

Table 2. Properties of opals and IOT samples prepared by infiltration method.

	IOT-156	IOT-247	IOT-320	IOT-493	IOT-292
D(voids of IOT)/nm	156	247	320	493	292
D(SiO$_2$)/nm	258	365	612	630	393
shrinkage/%	40	32	48	22	26
calculated λ_{IOT}/nm	349	553	716	1103	656
experimental λ_{IOT}/nm	ND	ND	ND	ND	647

ND—not detected.

In contrast to the infiltration method, the co-assembly has caused the formation of high quality of IOT samples, as shown in Figure 6. The IOT structures with pore sizes of 195 nm, 226 nm, and 246 nm can be successfully prepared from PS opals with diameters of 232 nm,

252 nm, and 278 nm, respectively (Table 3). However, IOT-280 sample, formed from the opal with largest PS particles (365 nm), has disordered array, presumably due to the high polydispersity (%PD) of the template (larger than recommended value of 5% [57,58]), as shown in Table 3. Other opals are characterized by relatively low %PD of PS particles, i.e., they are monodispersed. Hence, it has been confirmed that the homogeneity of particles forming opal is the key factor for the preparation of IOT films with a good quality. Moreover, it might be concluded that IOT-195, IOT-226, and IOT-246 are well-ordered FCC structure, as additionally confirmed by small values of FWHM (Table 3).
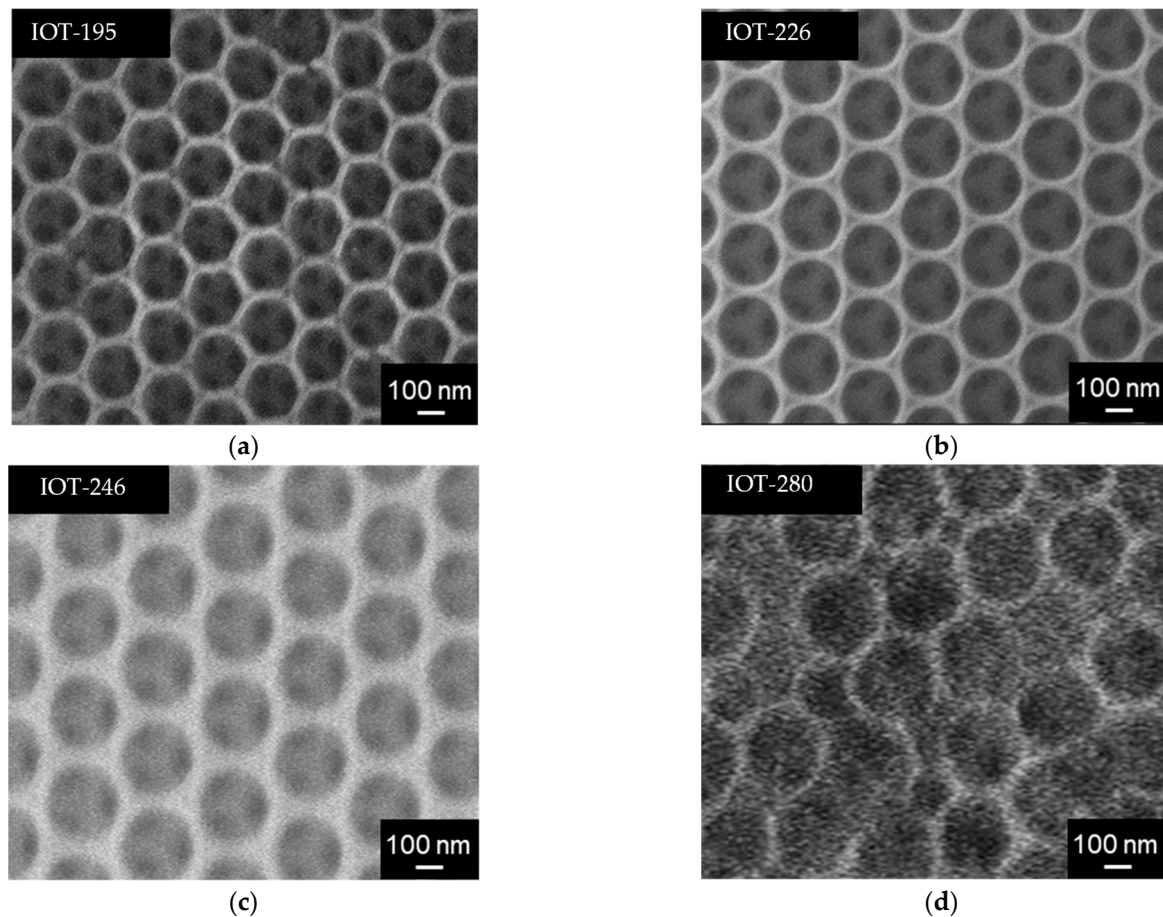
Figure 6. SEM images of: (**a**) IOT-195; (**b**) IOT-226; (**c**) IOT-246; (**d**) IOT-280.

Table 3. Summary of IOT-195, IOT-226, IOT-246, and IOT-280.

	IOT-195	IOT-226	IOT-246	IOT-280
D (PS)/nm	232	252	278	365
%PD of PS spheres	1.2	1.5	2.3	7.4
D (voids)/nm	195	226	246	280
shrinkage/%	16	10	12	23
λ_{opal}/nm	570	620	674	-
λ_{IOT}/nm	375	403	434	-
FWHM/nm	31	42	49	-
Thickness */μm	1.7	1.8	2	1.4

D—diameter of PS particles (first row) and voids (third row) in opal and inverse opal structures, respectively; * thickness measured by cross-section from SEM image.

3.3. Photocatalytic Activity

Photocatalytic activity of successfully prepared IOT samples, i.e., IOT-195, IOT-226, and IOT-246, was evaluated for oxidative decomposition of acetaldehyde gas under aerobic conditions. Figure 7a shows the transmission spectra for all samples together with an emission spectra of LED irradiation source. It should be reminded that titania is wide-bandgap semiconductor, and thus must be excited with UV light to form charge carriers. Accordingly, even though efficient light harvesting by tunning the PBG wavelength could be obtained, the activity at longer wavelengths than ca. 450 nm (385–400 nm in the case of pure defective-free titania, depending on its polymorphic form) is not expected.

(a)

(b)

(c)

(d)
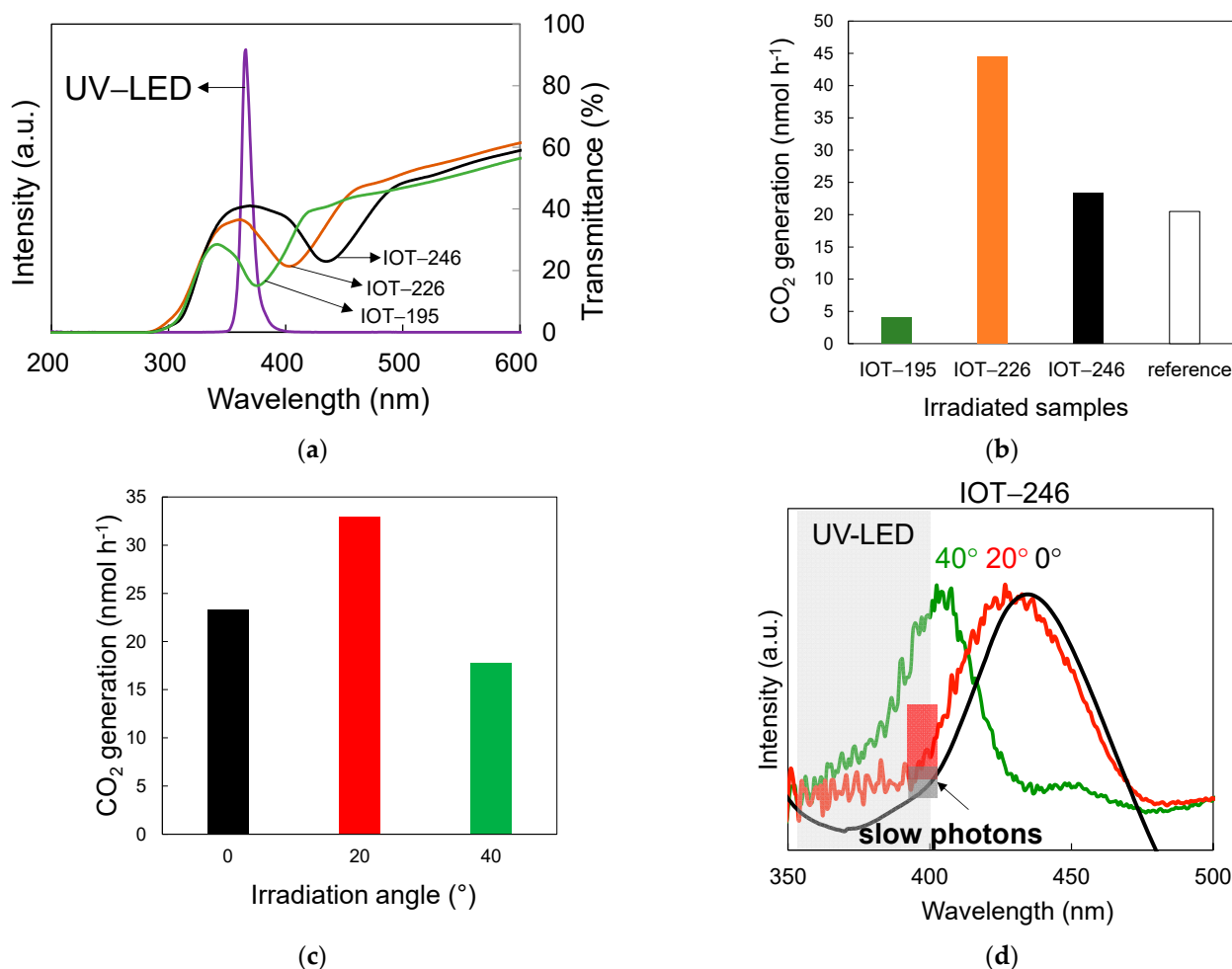
Figure 7. (**a**) Transmittance spectra of IOT samples and UV-LED emission peak; (**b**) the photocatalytic activity of IOT and reference (no PC) samples under irradiation at 0° angle; (**c**) the photocatalytic activity of IOT-246 sample under irradiation at different angles: 0°, 20°, and 40°; (**d**) extinction spectra of IOT-246 under different irradiation angle (0°, 20° and 40°) and UV-LED emission peak. The orange and blue squares represent the estimated slow photon effects for IOT-246 sample irradiated at 0° and 20°.

First, photocatalytic activity was investigated at 0° for three different IOTs and the reference (prepared from the mixture of PS particles of different sizes, and thus with no photonic properties—no PBG), and obtained data are shown in Figure 7b. It is clear that IOT-226 and IOT-246 have exhibited high photocatalytic activity in comparison to IOT-195. However, the photocatalytic activity of IOT-246 is only slightly higher than the reference sample (porous titania film without PBG). Hence, it is proposed that the slow photon effect is only hardly activated. In contrast, the activity of IOT-226 is more than twice higher than the reference. This could be explained by the matching of the LED emission, photoabsorption of titania ($\lambda < 400$ nm), and the slow photons arising at the blue

edges of their respective PBG peaks (Figure 7a). In contrast, the emission of LED matches with PBG wavelength for IOT-192 samples, and thus almost forbidden light penetration in the sample results in its worst activity. Interesting, the reference sample (no PBG) has exhibited much higher activity than IOT-195 (forbidden light penetration), but lower activity than other IOT materials. Accordingly, it has been confirmed that PCs structure could enhance photocatalytic performance by slow photon effect when the edges of PBG (not the wavelength of PBG) overlap with titania photoabsorption (and light emission).

To further study the impact of the slow photons on the photocatalytic activity, the angle dependence has been investigated, and thus IOT-246 sample has been irradiated at three different angles, i.e., $0°$, $20°$, and $40°$. The experimental PBG wavelengths for each irradiation position were 434, 426, and 405 nm (obtained from UV/vis spectra using a spectrophotometer with an angle tuning accessory), respectively. Interestingly, the sample has exhibited the highest photocatalytic activity when irradiated at $20°$, as shown in Figure 7c. In contrast, irradiation at $40°$ results in strong hypsochromic shift of PBG, and thus even a decrease in activity has been observed due to almost forbidden light penetration (Figure 7a,d). Although there is no undoubted evidence to explain these results, it is proposed that the precise overlapping of the slow photons arising at the blue edge of PBG wavelength of IOT, especially at $20°$ with LED irradiation at 365 nm might lead to the enhancement in light harvesting efficiency (Figure 7d), and thus enhanced photocatalytic activity. Interestingly, though the experimental PBG wavelength of IOT-226 (403 nm) is similar to IOT-246–40° (405 nm), the activity of IOT-246–40° is not as high as IOT-226, which could be caused by that loss of photon flux on the IOT film. The further experiments on the explanation of this aspect are under study.

4. Summary and Conclusions

The fabrication of opal and inverse opal structures with different photonic properties have been succeeded via sandwich-vacuum-assisted infiltration and co-assembly methods. The opals of high quality (built of silica or PS) could be obtained by both methods. However, the co-assembly is more recommended for IOT formation since the infiltration method results mostly in the formation of IOT with large content of defects, cracks, and titania overlayers. It has been found that PBG wavelength for both opals and inverse opals depends on the size of particles and voids, respectively, as well as the irradiation angle, which could be useful for the design of novel materials with controlled photonic properties.

The photocatalytic activity study has indicated that the perfect matching of photoabsorption property of material (here titania), the irradiation wavelength and the slow photon wavelength might result in significant enhancement of photocatalytic activity. Interestingly, the further tuning in the aspect of irradiation angle could vary the position of PBG (also the slow photon effect). Hence, the optimal angle of irradiation to overlap with photoabsorption of material and irradiation source could enhance the photochemical reactions. Accordingly, it has been found that IOT-246 irradiated at $20°$ exhibits the best performance, presumably due to the wavelength overlapping between LED emission and slow photon effects, tuned by incident angle. Based on the results of size dependent activity and angle dependent activity, the optimized PBG wavelength of IOT is between 403 and 434 nm. However, it must also be pointed out that the use of other irradiation sources with emission at longer wavelengths to match the red edge of PBG (slow photons) is not recommended as bare titania cannot be excited by photons with energy lower than ca. 3.0 eV (only "trapped" photons inside the structure but without any photocatalytic effect). The further research to clarify this aspect is now under study.

Author Contributions: Conceptualization, E.K.; methodology, T.R.M., M.T., B.O. and E.K.; investigation, L.W.; resources, B.O. and E.K.; writing—original draft preparation, L.W., T.R.M. and E.K.; writing—review and editing, L.W. and E.K.; visualization, L.W. and K.W.; supervision, M.T., B.O. and E.K.; funding acquisition, B.O. and E.K. All authors have read and agreed to the published version of the manuscript.

Conflicts of Interest: The authors declare no conflict of interest.

References

1. Roy, N.; Suzuki, N.; Terashima, C.; Fujishima, A. Recent Improvements in the Production of Solar Fuels: From CO_2 Reduction to Water Splitting and Artificial Photosynthesis. *Bull. Chem. Soc. Jpn.* **2019**, *92*, 178–192. [CrossRef]
2. Abe, R. Recent progress on photocatalytic and photoelectrochemical water splitting under visible light irradiation. *J. Photochem. Photobiol. C* **2010**, *11*, 179–209. [CrossRef]
3. Hoffmann, M.R.; Martin, S.T.; Choi, W.Y.; Bahnemann, D.W. Environmental applications of semiconductor photocatalysis. *Chem. Rev.* **1995**, *95*, 69–96. [CrossRef]
4. Serpone, N.; Borgarello, E.; Pelizzetti, E. Photoreduction and photodegradation of inorganic pollutants: II. Selective reduction and recovery of Au, Pt, Pd, Rh, Hg, and Pb. *NATO ASI Ser. Ser. C Math. Phys. Sci.* **1988**, *237*, 527–565.
5. Markowska-Szczupak, A.; Ulfig, K.; Morawski, W.A. The application of titanium dioxide for deactivation of bioparticulates: An overview. *Catal. Today* **2011**, *161*, 249–257. [CrossRef]
6. Sakai, N.; Fujiwara, Y.; Takahashi, Y.; Tatsuma, T. Plasmon-resonance-based generation of cathodic photocurrent at electrode-posited gold nanoparticles coated with TiO2 films. *Chem. Phys. Chem.* **2009**, *10*, 766–769. [CrossRef]
7. Berger, T.; Sterrer, M.; Diwald, O.; Knozinger, E.; Panayotov, D.; Thompson, T.L.; Yates, J.T., Jr. Light-induced charge separation in anatase TiO_2 particles. *J. Phys. Chem. B* **2005**, *109*, 6061–6068. [CrossRef]
8. Rothenberger, G.; Moser, J.; Gratzel, M.; Serpone, N.; Sharmaf, D.K. Charge carrier trapping and recombination dynamics in small semiconductor particles. *J. Am. Chem. Soc.* **1985**, *107*, 8054–8059. [CrossRef]
9. Asahi, R.; Morikawa, T.; Ohwaki, T.; Aoki, K.; Taga, Y. Visible-light photocatalysis in nitrogen-doped titanium oxides. *Science* **2001**, *293*, 269–271. [CrossRef]
10. Ohno, T.; Mitsui, T.; Matsumura, M. Photocatalytic activity of S-doped TiO_2 photocatalyst under visible light. *Chem. Lett.* **2003**, *32*, 364–365. [CrossRef]
11. Zaleska, A. Doped-TiO_2: A review. *Rec. Pat. Eng.* **2008**, *2*, 157–164. [CrossRef]
12. Tryba, B.; Tsumura, T.; Janus, M.; Morawski, A.W.; Inagaki, M. Carbon-coated anatase: Adsorption and decomposition of phenol in water. *Appl. Catal. B: Environ.* **2004**, *50*, 177–183. [CrossRef]
13. Kowalska, E.; Remita, H.; Colbeau-Justin, C.; Hupka, J.; Belloni, J. Modification of titanium dioxide with platinum ions and clusters: Application in photocatalysis. *J. Phys. Chem. C* **2008**, *112*, 1124–1131. [CrossRef]
14. Kouame, N.A.; Alaoui, O.T.; Herissan, A.; Larios, E.; Jose-Yacaman, M.; Etcheberry, A.; Colbeau-Justin, C.; Remita, H. Visible light-induced photocatalytic activity of modified titanium(IV) oxide with zero-valent bismuth clusters. *New J. Chem.* **2015**, *39*, 2316–2322. [CrossRef]
15. Wang, K.; Bielan, Z.; Endo-Kimura, M.; Janczarek, M.; Zhang, D.; Kowalski, D.; Zielińska-Jurek, A.; Markowska-Szczupak, A.; Ohtani, B.; Kowalska, E. On the mechanism of photocatalytic reactions on $Cu_xO@TiO_2$ core–shell photocatalysts. *J. Mater. Chem. A* **2021**, *9*, 10135–10145. [CrossRef]
16. Endo-Kimura, M.; Janczarek, M.; Bielan, Z.; Zhang, D.; Wang, K.; Markowska-Szczupak, A.; Kowalska, E. Photocatalytic and antimicrobial properties of Ag_2O/TiO_2 heterojunction. *ChemEngineering* **2019**, *3*, 3. [CrossRef]
17. Janczarek, M.; Endo, M.; Zhang, D.; Wang, K.; Kowalska, E. Enhanced photocatalytic and antimicrobial prformance of cuprous oxide/titania: The effect of titania matrix. *Materials* **2018**, *11*, 2069. [CrossRef]
18. Tabata, M.; Maeda, K.; Higashi, M.; Lu, D.L.; Takata, T.; Abe, R.; Domen, K. Modified Ta3N5 Powder as a Photocatalyst for O-2 Evolution in a Two-Step Water Splitting System with an Iodate/Iodide Shuttle Redox Mediator under Visible Light. *Langmuir* **2010**, *26*, 9161–9165. [CrossRef]
19. Yashima, M.; Maeda, K.; Teramura, K.; Takata, T.; Domen, K. Crystal structure and optical properties of $(Ga_{1-x} Zn_x)(N_{1-x}O_x)$ oxynitride photocatalyst (x = 0.13). *Chem. Phys. Lett.* **2005**, *416*, 225–228. [CrossRef]
20. Ishikawa, A.; Takata, T.; Kondo, J.N.; Hara, M.; Kobayashi, H.; Domen, K. Oxysulfide $Sm_2Ti_2S_2O_5$ as a stable photocatalyst for water oxidation and reduction under visible light irradiation (λ > 650 nm). *J. Am. Chem. Soc.* **2002**, *124*, 13547–13553. [CrossRef]
21. Suzuki, H.; Higashi, M.; Tomita, O.; Ishii, Y.; Yamamoto, T.; Kato, D.; Kotani, T.; Ozaki, D.; Nozawa, S.; Nakashima, K.; et al. $PbBi_3O_4X_3$ (X = Cl, Br) with Single/Double Halogen Layers as a Photocatalyst for Visible-Light-Driven Water Splitting: Impact of a Halogen Layer on the Band Structure and Stability. *Chem. Mater.* **2021**, *33*, 9580–9587. [CrossRef]
22. Ogawa, K.; Suzuki, H.; Zhong, C.; Sakamoto, R.; Tomita, O.; Saeki, A.; Kageyama, H.; Abe, R. Layered Perovskite Oxyiodide with Narrow Band Gap and Long Lifetime Carriers for Water Splitting Photocatalysis. *J. Am. Chem. Soc.* **2021**, *143*, 8446–8453. [CrossRef] [PubMed]
23. Sasaki, Y.; Nemoto, H.; Saito, K.; Kudo, A. Solar Water Splitting Using Powdered Photocatalysts Driven by Z-Schematic Interparticle Electron Transfer without an Electron Mediator. *J. Phys. Chem. C* **2009**, *113*, 17536–17542. [CrossRef]
24. Zhang, D.; Mao, B.; Li, D.; Liu, Y.; Li, F.; Dong, W.; Jiang, T.; Shi, W. 0D/2D Z-scheme heterojunctions of Zn-$AgIn_5S_8$ QDs/α-Fe_2O_3 nanosheets for efficient visible-light-driven hydrogen production. *Chem. Eng. J.* **2021**, *417*, 128275–128284. [CrossRef]

25. Nakada, A.; Kuriki, R.; Sekizawa, K.; Nishioka, S.; Vequizo, J.J.M.; Uchiyama, T.; Kawakami, N.; Lu, D.L.; Yamakata, A.; Uchimoto, Y.; et al. Effects of interfacial electron transfer in metal complex-semiconductor hybrid photocatalysts on Z-scheme CO_2 reduction under visible light. *ACS Catal.* **2018**, *8*, 9744–9754. [CrossRef]

26. Chang, X.; Wang, T.; Zhang, P.; Zhang, J.; Li, A.; Gong, J. Enhanced Surface Reaction Kinetics and Charge Separation of p–n Heterojunction $Co_3O_4/BiVO_4$ Photoanodes. *J. Am. Chem. Soc.* **2015**, *137*, 8356–8359. [CrossRef] [PubMed]

27. Ohtani, B. Photocatalysis A to Z-What we know and what we do not know in a scientific sense. *J. Photochem. Photobiol. C* **2010**, *11*, 157–178. [CrossRef]

28. Ogawa, K.; Sakamoto, R.; Zhong, C.; Suzuki, H.; Kato, K.; Tomita, O.; Nakashima, K.; Yamakata, A.; Tachikawa, T.; Saeki, A.; et al. Manipulation of charge carrier flow in Bi_4NbO_8Cl nanoplate photocatalyst with metal loading. *Chem. Sci.* **2022**, *13*, 3118–3128. [CrossRef]

29. Janczarek, M.; Kowalska, E.; Ohtani, B. Decahedral-shaped anatase titania photocatalyst particles: Synthesis in a newly developed coaxial-flow gas-phase reactor. *Chem. Eng. J.* **2016**, *289*, 502–512. [CrossRef]

30. Wei, Z.; Janczarek, M.; Endo, M.; Wang, K.L.; Balcytis, A.; Nitta, A.; Mendez-Medrano, M.G.; Colbeau-Justin, C.; Juodkazis, S.; Ohtani, B.; et al. Noble metal-modified faceted anatase titania photocatalysts: Octahedron versus decahedron. *Appl Catal B-Environ.* **2018**, *237*, 574–587. [CrossRef]

31. Kowalski, D.; Kim, D.; Schmuki, P. TiO_2 nanotubes, nanochannels and mesosponge: Self-organized formation and applications. *Nano Today* **2013**, *8*, 235–264. [CrossRef]

32. Janczarek, M.; Wei, Z.; Mogan, T.R.; Wang, L.; Wang, K.; Nitta, A.; Ohtani, B.; Kowalska, E. Does Symmetry Control Photocatalytic Activity of Titania-Based Photocatalysts? *Symmetry* **2021**, *13*, 1682. [CrossRef]

33. Belloni, J.; Treguer, M.; Remita, H.; De Keyzer, R. Enhanced yield of photoinduced electrons in doped silver halide crystals. *Nature* **1999**, *402*, 865–867. [CrossRef]

34. Curti, M.; Mendive, C.B.; Grela, M.A.; Bahnemann, D.W. Stopband tuning of TiO_2 inverse opals for slow photon absorption. *Mater. Res. Bull.* **2017**, *91*, 155–165. [CrossRef]

35. Raja-Mogan, T.; Lehoux, A.; Takashima, M.; Kowalska, E.; Ohtani, B. Slow photon-induced enhancement of photocatalytic activity of gold nanoparticle-incorporated titania in-verse opal. *Chem. Lett.* **2021**, *50*, 711–713. [CrossRef]

36. Raja-Mogan, T.; Ohtani, B.; Kowalska, E. Photonic crystals for plasmonic photocatalysis. *Catalysts* **2020**, *10*, 827. [CrossRef]

37. Lopez, C. Materials aspects of photonic crystals. *Adv. Mater.* **2003**, *15*, 1679–1704. [CrossRef]

38. Richel, A.; Johnson, N.P.; McComb, D.W. Observation of Bragg reflection in photonic crystals synthesized from air spheres in a titania matrix. *Appl. Phys. Lett.* **2000**, *76*, 1816–1818. [CrossRef]

39. Yablonovitch, E. Photonic Band-Gap Structures. *J. Opt. Soc. Am. B* **1993**, *10*, 283–295. [CrossRef]

40. Yablonovitch, E. Inhibited Spontaneous Emission in Solid-State Physics and Electronics. *Phys. Rev. Lett.* **1987**, *58*, 2059–2062. [CrossRef]

41. John, S. Strong localization of photons in certain disordered dielectric superlattices. *Phys. Rev. Lett.* **1987**, *58*, 2486–2489. [CrossRef]

42. Wang, K.L.; Janczarek, M.; Wei, Z.S.; Raja-Mogan, T.; Endo-Kimura, M.; Khedr, T.M.; Ohtani, B.; Kowalska, E. Morphology- and crystalline composition-governed activity of titania-based photocatalysts: Overview and perspective. *Catalysts* **2019**, *9*, 1054. [CrossRef]

43. Ohtani, B.; Mahaney, O.O.P.; Amano, F.; Murakami, N.; Abe, R. What Are Titania Photocatalysts?-An Exploratory Correlation of Photocatalytic Activity with Structural and Physical Properties. *J. Adv. Oxid. Technol.* **2010**, *13*, 247–261. [CrossRef]

44. Nakata, K.; Fujishima, A. TiO_2 photocatalysis: Design and applications. *J. Photochem. Photobiol. C* **2012**, *13*, 169–189. [CrossRef]

45. Chiang, C.C.; Tuyen, L.D.; Ren, C.R.; Chau, L.K.; Wu, C.Y.; Huang, P.J.; Hsu, C.C. Fabrication of titania inverse opals by multi-cycle dip-infiltration for optical sensing. *Photonic Nanostruct.* **2016**, *19*, 48–54. [CrossRef]

46. Wu, M.; Jin, J.; Liu, J.; Deng, Z.; Li, Y.; Deparis, O.; Su, B.-L. High photocatalytic activity enhancement of titania inverse opal films by slow photon effect induced strong light absorption. *J. Mater. Chem. A* **2013**, *1*, 15491–15500. [CrossRef]

47. Cai, Z.; Xiong, Z.; Lu, X.; Teng, J. In situ gold-loaded titania photonic crystals with enhanced photocatalytic activity. *J. Mater. Chem. A* **2014**, *2*, 545–553. [CrossRef]

48. Liu, W.; Zou, B.; Zhao, J.; Cui, H. Optimizing sol–gel infiltration for the fabrication of high-quality titania inverse opal and its photocatalytic activity. *Thin Solid Films* **2010**, *518*, 4923–4927. [CrossRef]

49. Cai, Z.; Teng, J.; Xiong, Z.; Li, Y.; Li, Q.; Lu, X.; Zhao, X.S. Fabrication of TiO_2 Binary Inverse Opals without Overlayers via the Sandwich-Vacuum Infiltration of Precursor. *Langmuir* **2011**, *27*, 5157–5164. [CrossRef]

50. Maji, D.; Lahiri, S.K.; Das, S. Study of hydrophilicity and stability of chemically modified PDMS surface using piranha and KOH solution. *Surf. Interface Anal.* **2012**, *44*, 62–69. [CrossRef]

51. Bogush, G.H.; Tracy, M.A.; Zukoski, C.F. Preparation of monodisperse silica particles: Control of size and mass fraction. *J. Non Cryst. Solids* **1988**, *104*, 95–106. [CrossRef]

52. Phillips, K.R.; Shirman, T.; Shirman, E.; Shneidman, A.V.; Kay, T.M.; Aizenberg, J. Nanocrystalline Precursors for the Co-Assembly of Crack-Free Metal Oxide Inverse Opals. *Adv. Mater.* **2018**, *30*, 1706329. [CrossRef] [PubMed]

53. Jovic, V.; Idriss, H.; Waterhouse, G.I.N. Slow photon amplification of gas-phase ethanol photo-oxidation in titania inverse opal photonic crystals. *Chem. Phys.* **2016**, *479*, 109–121. [CrossRef]

54. Sordello, F.; Duca, C.; Maurino, V.; Minero, C. Photocatalytic metamaterials: TiO_2 inverse opals. *Chem. Commun.* **2011**, *47*, 6147–6149. [CrossRef]

55. Wu, M.; Liu, J.; Jin, J.; Wang, C.; Huang, S.Z.; Deng, Z.; Li, Y.; Su, B.L. Probing significant light absorption enhancement of titania inverse opal films for highly exalted photocatalytic degradation of dye pollutants. *Appl. Catal. B-Environ.* **2014**, *150*, 411–420. [CrossRef]

56. Lu, Y.; Yu, H.T.; Chen, S.; Quan, X.; Zhao, H.M. Integrating plasmonic nanoparticles with TiO$_2$ photonic crystal for enhancement of visible-light-driven photocatalysis. *Environ. Sci. Technol.* **2012**, *46*, 1724–1730. [CrossRef]

57. Jiang, P.; Bertone, J.F.; Hwang, K.S.; Colvin, V.L. Single-crystal colloidal multilayers of controlled thickness. *Chem. Mater.* **1999**, *11*, 2132–2140. [CrossRef]

58. Mayoral, R.; Requena, J.; Moya, J.S.; Lopez, C.; Cintas, A.; Miguez, H.; Meseguer, F.; Vazquez, L.; Holgado, M.; Blanco, A. 3D long-range ordering in an SiO$_2$ submicrometer-sphere sintered superstructure. *Adv. Mater.* **1997**, *9*, 257–260. [CrossRef]